



Supporting Information

© Wiley-VCH 2012

69451 Weinheim, Germany

DNA Origami Gatekeepers for Solid-State Nanopores**

Ruoshan Wei, Thomas G. Martin, Ulrich Rant, and Hendrik Dietz**

anie_201200688_sm_miscellaneous_information.pdf

Guide to the Supporting Information

- 3 **Note S1:** **Assembly and quality control of DNA nanoplates**
(Figs. S1-S5: Scaffold/Staple design layout for DNA nanoplates)
(Figs. S6-S9: Negative stain TEM micrographs of DNA nanoplates)
- 13 **Note S2:** **SiN nanopore fabrication and experimental methods**
- 15 **Note S3:** **Current noise analysis**
(incl. Fig. S10, equation S1)
- 17 **Note S4:** **Influence of nanopore diameter and orientation on nanoplate capture, nanopore arrays**
(incl. Fig. S11, S12)
- 18 **Note S5:** **Conductance of the DNA nanoplate on SiN nanopore hybrid**
(incl. Fig. S13, equations S2-S8)
- 20 **Note S6:** **Analysis of streptavidin translocations**
(incl. Fig. S14)
- 21 **Note S7:** **Analysis of dsDNA translocations**
(incl. Fig. S15)
- 22 **Note S8:** **DNA nanoplate without central aperture**
(incl. Fig. S16)
- 23 **Note S9:** **M13mp18 genomic DNA in a nanoplate without bait motif**
(incl. Fig. S17)
- 24 **Note S10:** **M13mp18 genomic DNA in a nanoplate with multiple baits**
(incl. Fig. S18)
- 25 **Note S11:** **M13mp18 genomic DNA in a nanoplate: dwell time analysis**
(incl. Fig. S19, equations S9, S10)
- 27 **Note S12:** **Supporting references**
- 28 **Note S13:** **Sequence infomation**

Note S1: Assembly and quality control of DNA nanoplates

Molecular self-assembly with scaffolded DNA origami.

Structures were designed using caDNAno v.02 [1]. Recombinant M13 filamentous bacteriophage of length 8064 bases were prepared as previously described [2]. Staple oligonucleotide strands were prepared by solid-phase chemical synthesis (Eurofins MWG, Ebersberg, Germany, HPSF purification). Production of DNA nanoplate structures was accomplished as previously described [2, 3] in one-pot reactions by mixing 20 nM scaffold strands derived from M13 bacteriophage with 100 nM of oligonucleotide staple strands in a buffer including 5 mM TRIS, 1 mM EDTA, 18 mM MgCl₂, 5 mM NaCl (pH 8). The mixture was subjected to thermal-annealing ramps that cooled from 65°C to 25°C over the course of minimum two or up to four days.

Gel purification.

Reaction products were electrophoresed on 2% agarose gels containing 0.5x TBE, 11 mM MgCl₂, 0.5 µg/ml ethidium bromide at 70V for four hours in a gel box incubated in an ice water bath. Target bands were excised and DNA recovered by physical extraction by centrifugation for 10 min at 13000 rcf at 4°C in Freeze’N’Squeeze DNA gel extraction spin columns (Bio Rad). Recovered material in the flow through was quality-controlled by direct imaging by negative stain transmission electron microscopy and stored at 4°C for further use.

Transmission electron microscopy.

Particles were adsorbed on glow-discharged formvar-supported carbon-coated Cu400 TEM grids and stained using a 2% aqueous uranyl formate solution containing 25 mM NaOH. Imaging was performed using a Philips CM100 electron microscopy operated at 100 kV. Images were acquired using a AMT 4x4 Megapixel CCD camera. Micrograph scale bars were calibrated using 2D catalase crystal lattice constants as length reference. Imaging was performed at 28500x magnification.

Image processing.

Micrographs of individual particles were picked using the EMAN2 [4] boxer routine. Micrograph alignment and superposition was performed using IMAGIC (Image Science, Berlin).

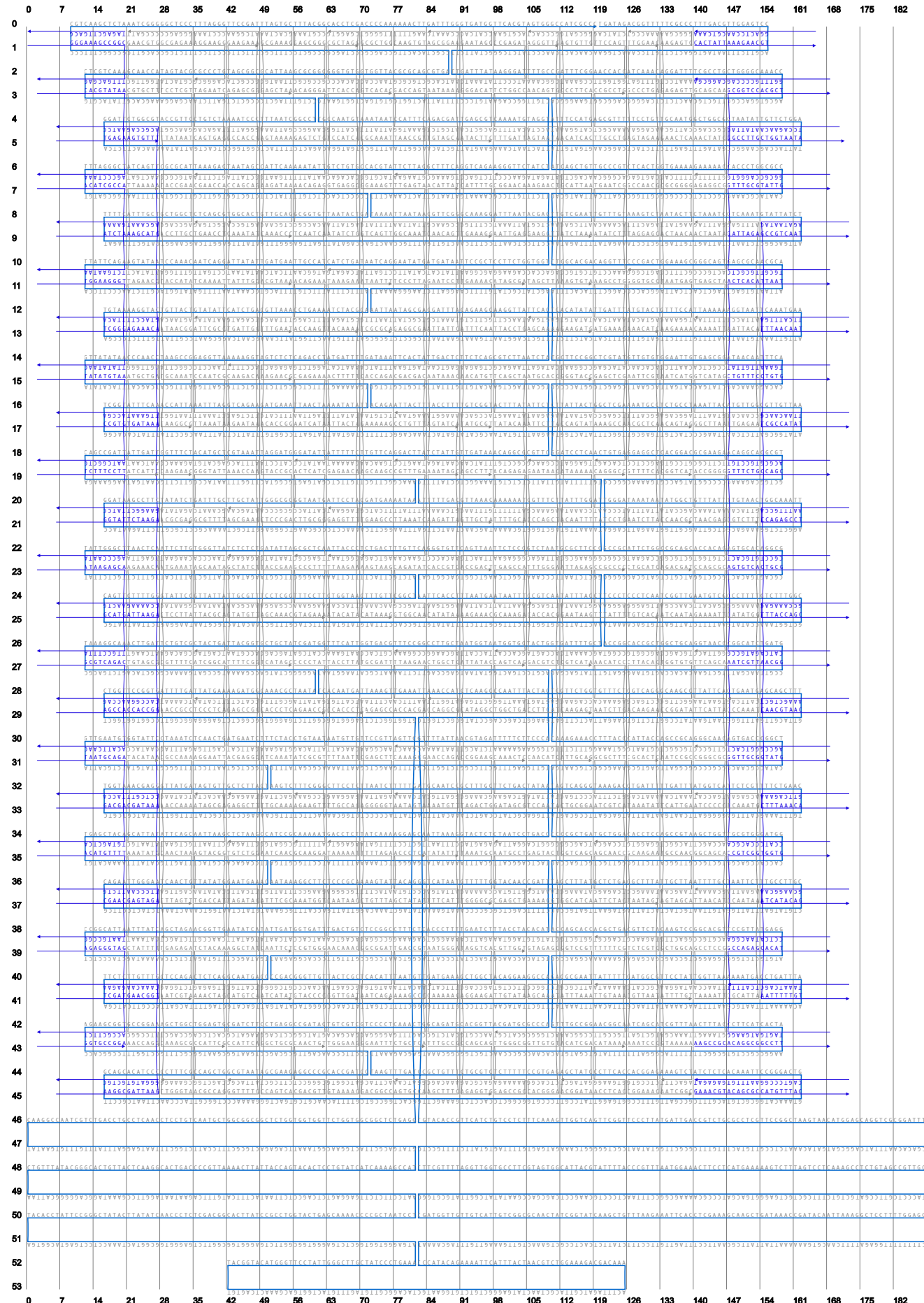


Fig. S1: Scaffold / staple layout diagram for DNA nanoplate plate lacking any aperture. Generated with cadnano v0.2 Grey strands = core, blue strands = poly T interface passivation.

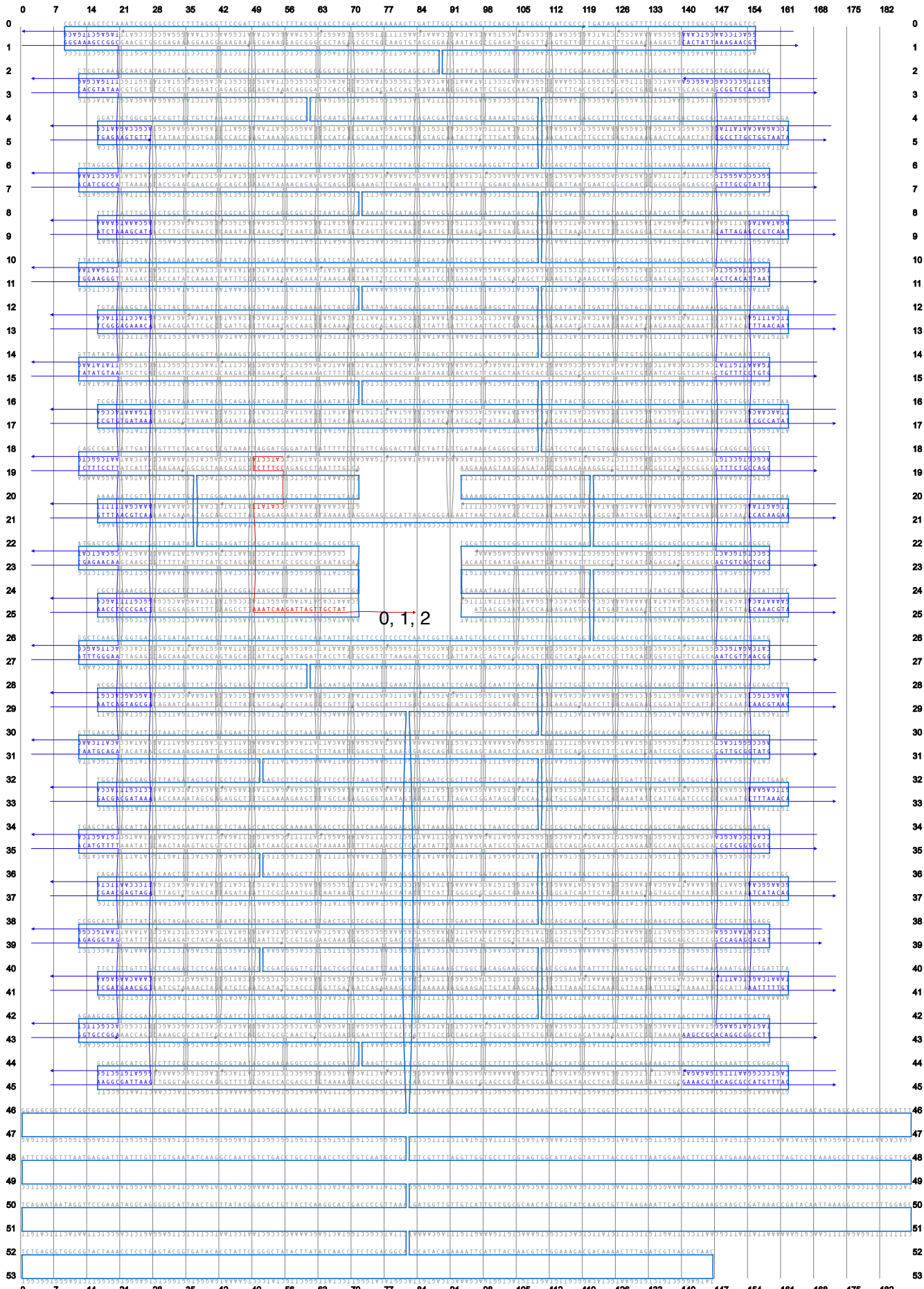
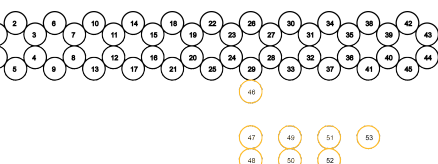


Fig. S2: Scaffold / staple layout diagram for DNA nanoplate with 5nm x 7nm aperture and a single bait motif. Generated with cadnano v0.2. Grey strands = core, blue strands = poly T interface passivation, red strand includes 3' bait overhang (0 = void, 1=TTTAATT, 2=TTTCCGG). Loop can be made double-stranded using additional staples (see note S13).



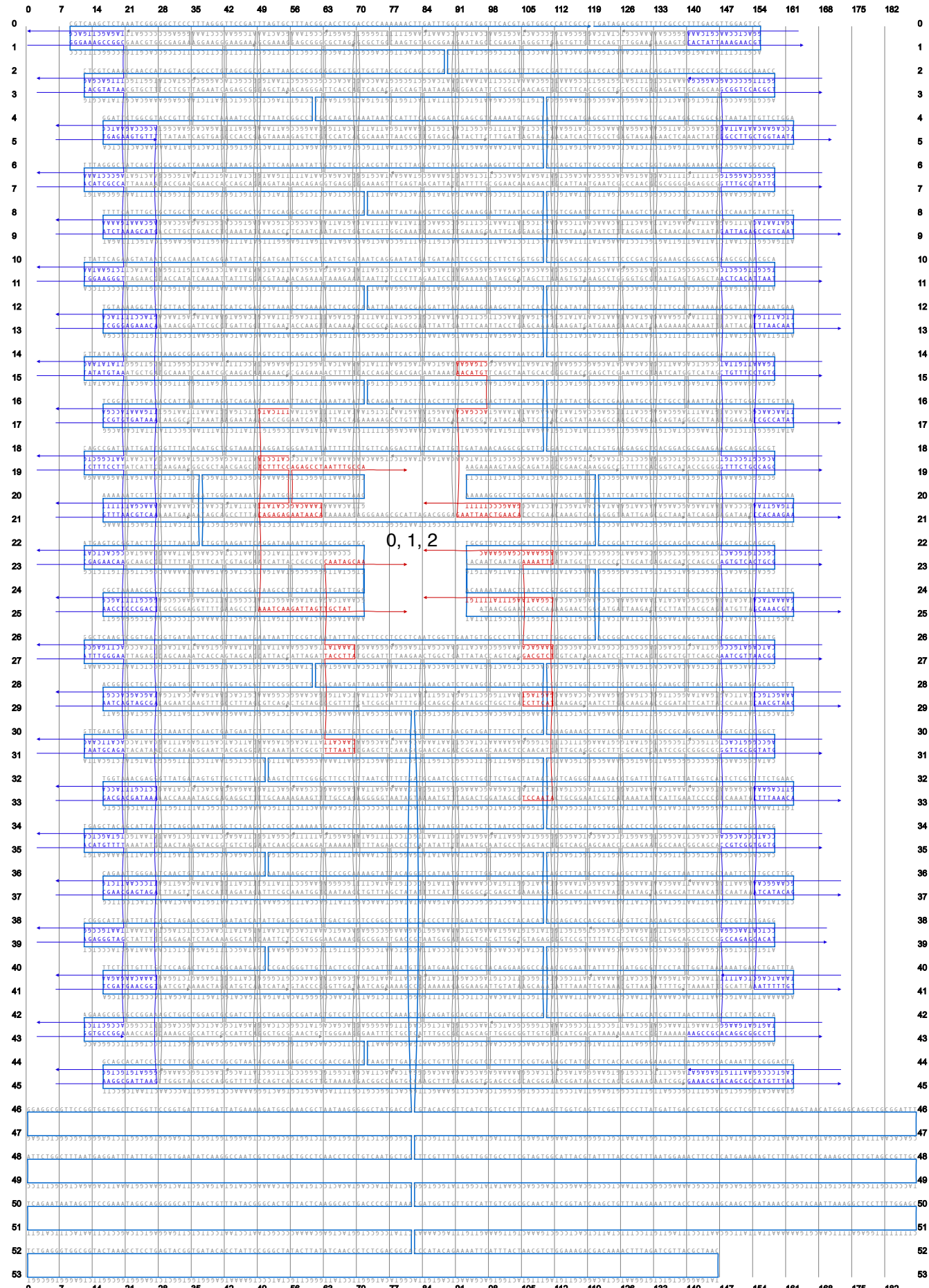


Fig. S3: Scaffold / staple layout diagram for DNA nanoplates with 5nm x 7nm aperture carrying six copies of a bait motif. Generated with cadnano v0.2 Grey strands = core, blue strands = poly T interface passivation, red strands include 3' bait overhang (0 = void, 1=TTTAATT, 2=TTTCCGG).

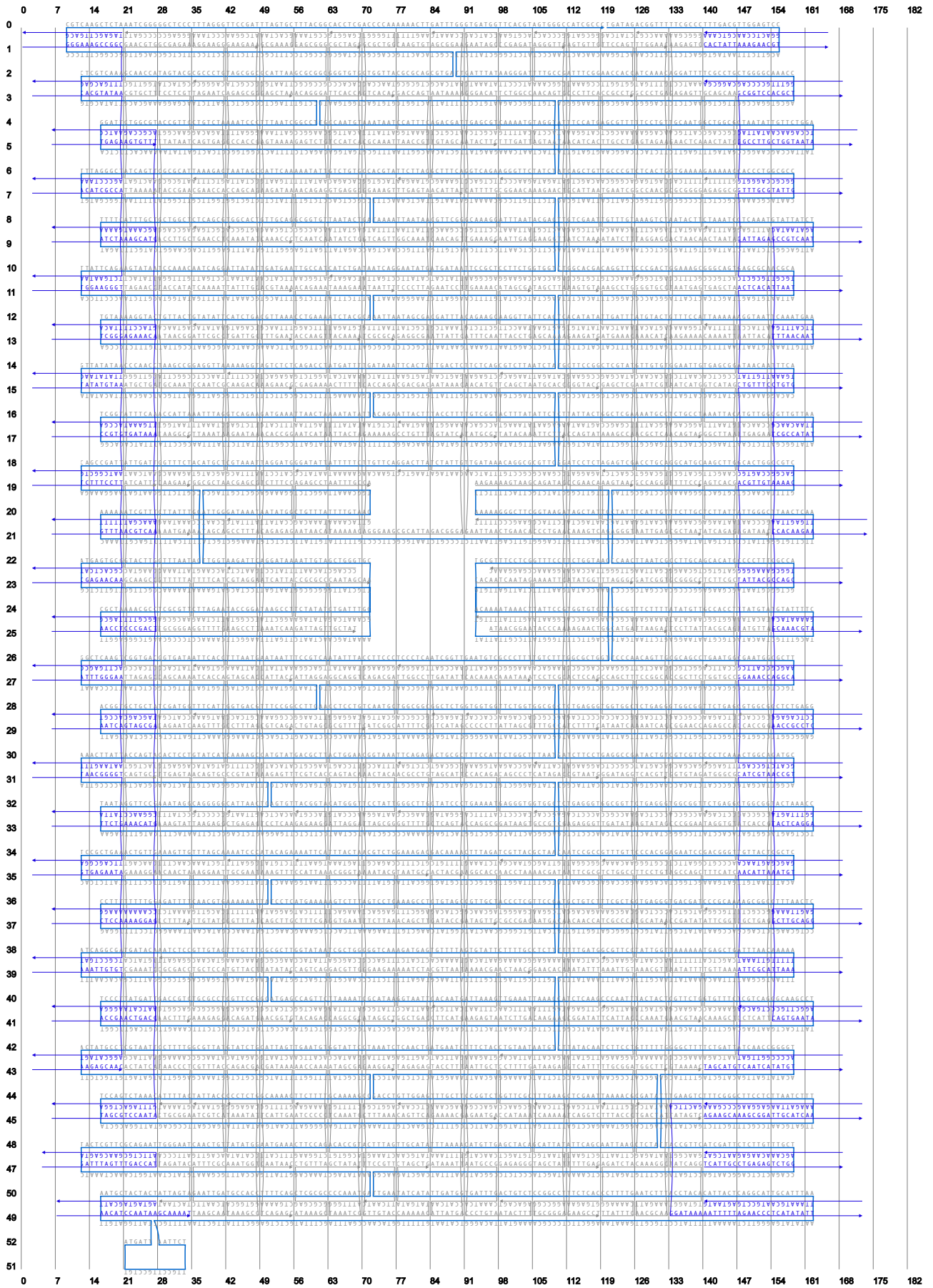


Fig. S4: Scaffold / staple layout diagram for DNA nanoplate with 5nm x 7nm aperture lacking a flexible loop. Generated with cadnano v0.2. Grey strands = core, blue strands = poly T interface passivation.



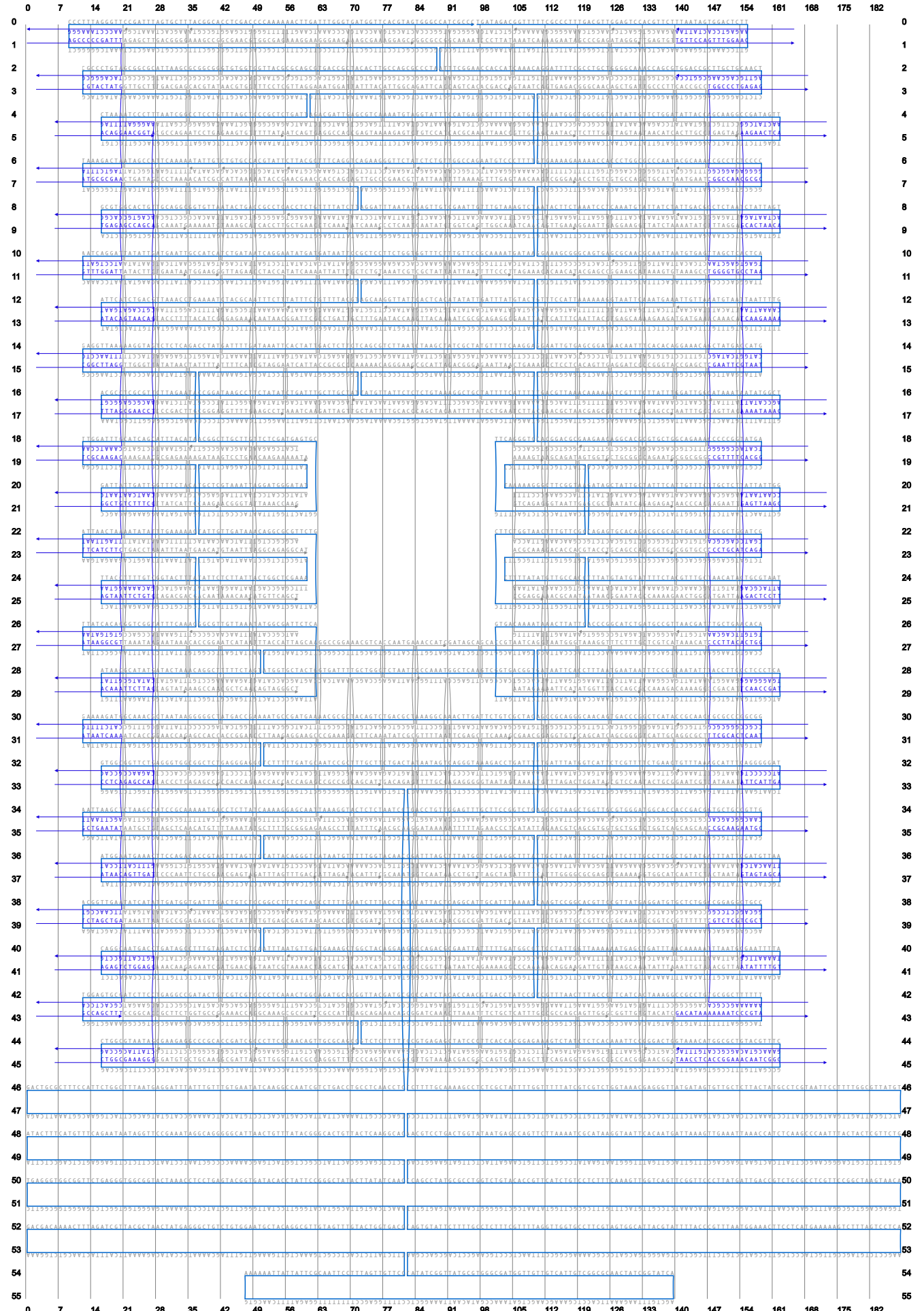
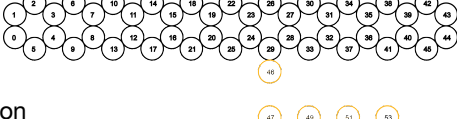


Fig. S5: Scaffold / staple layout diagram for DNA nanoplate with 9nm x 14nm aperture. Generated with cadnano v0.2. Grey strands = core, blue strands = poly T interface passivation.



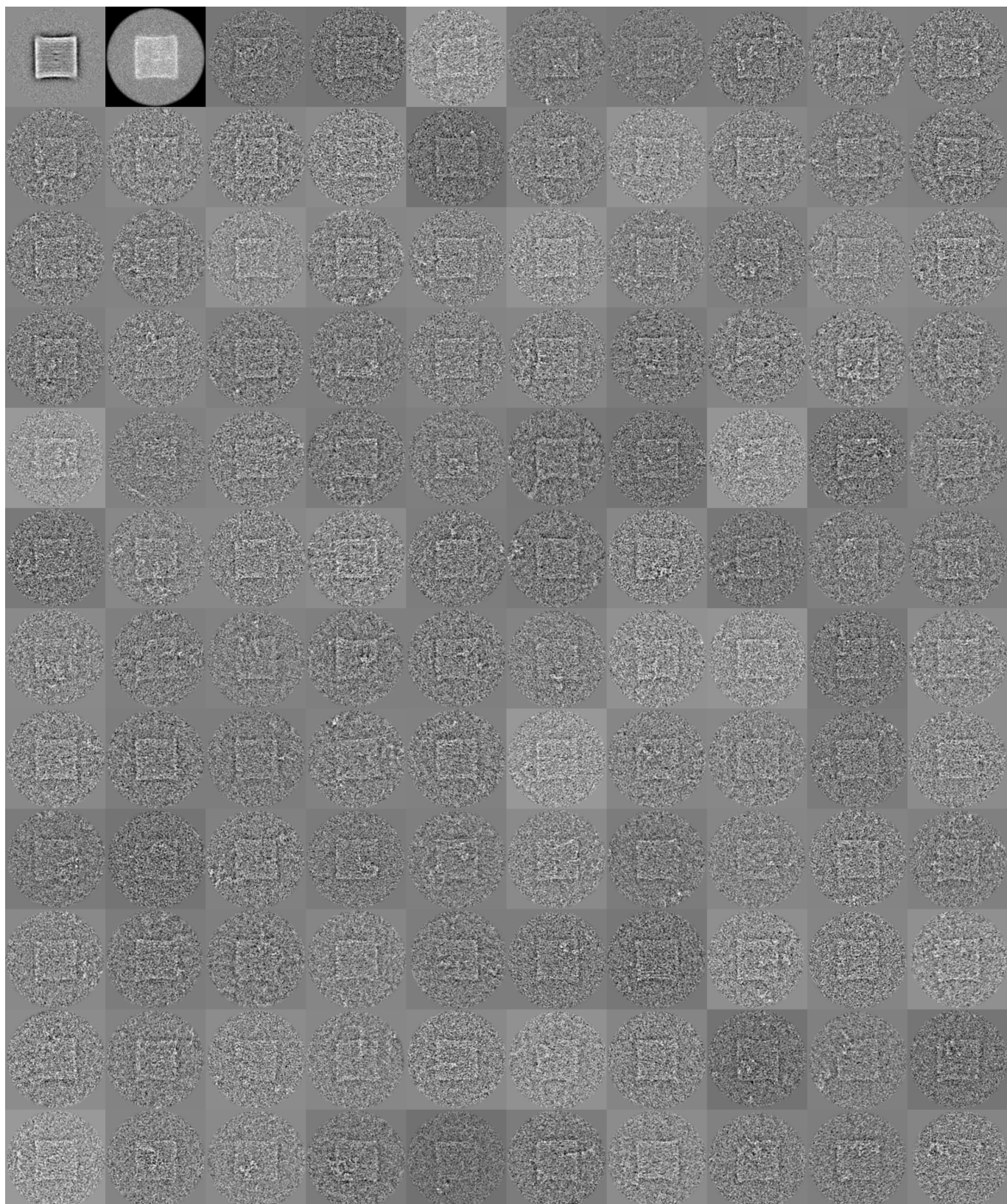


Fig. S6:

Negative-stain TEM micrographs of DNA nanoplate lacking any aperture. The flexible loop assumes random shapes and orientations relative to the gatekeeper plate. However, it always protrudes near the center of the nanoplate, thus explaining the dark spots in the average image (#1). Scale of each micrograph: 125nm x 125nm. Top row, image #1 = average micrograph; image #2 = variance micrograph computed from the shown library of micrographs.

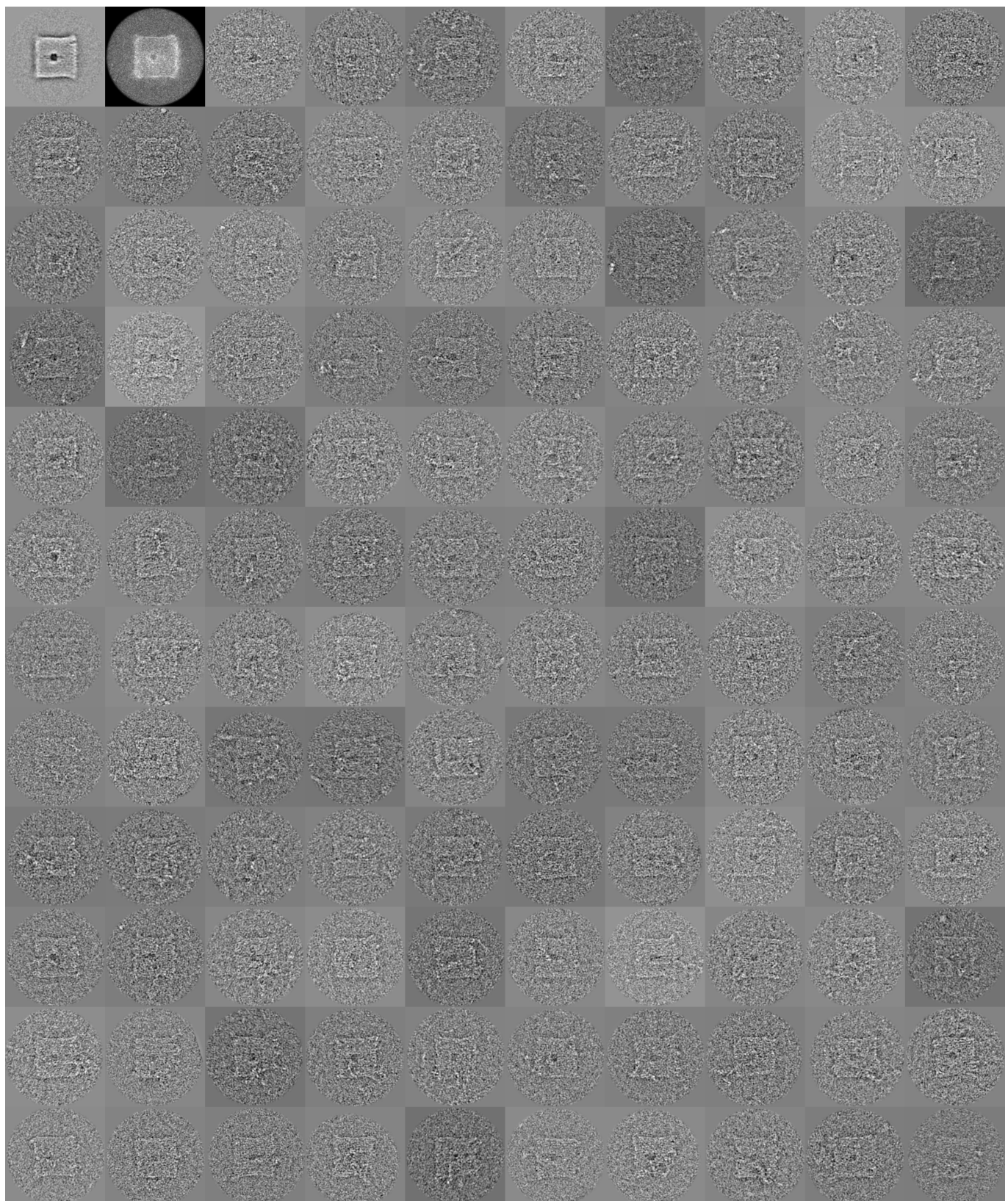


Fig. S7:

Negative-stain TEM micrographs of DNA nanoplate with 5nm x 7nm aperture. The flexible loop occurs in random orientations relative to the gatekeeper plate. Scale of each micrograph: 125nm x 125nm. Top row, image #1 = average micrograph; image #2 = variance micrograph computed from the shown library of micrographs.

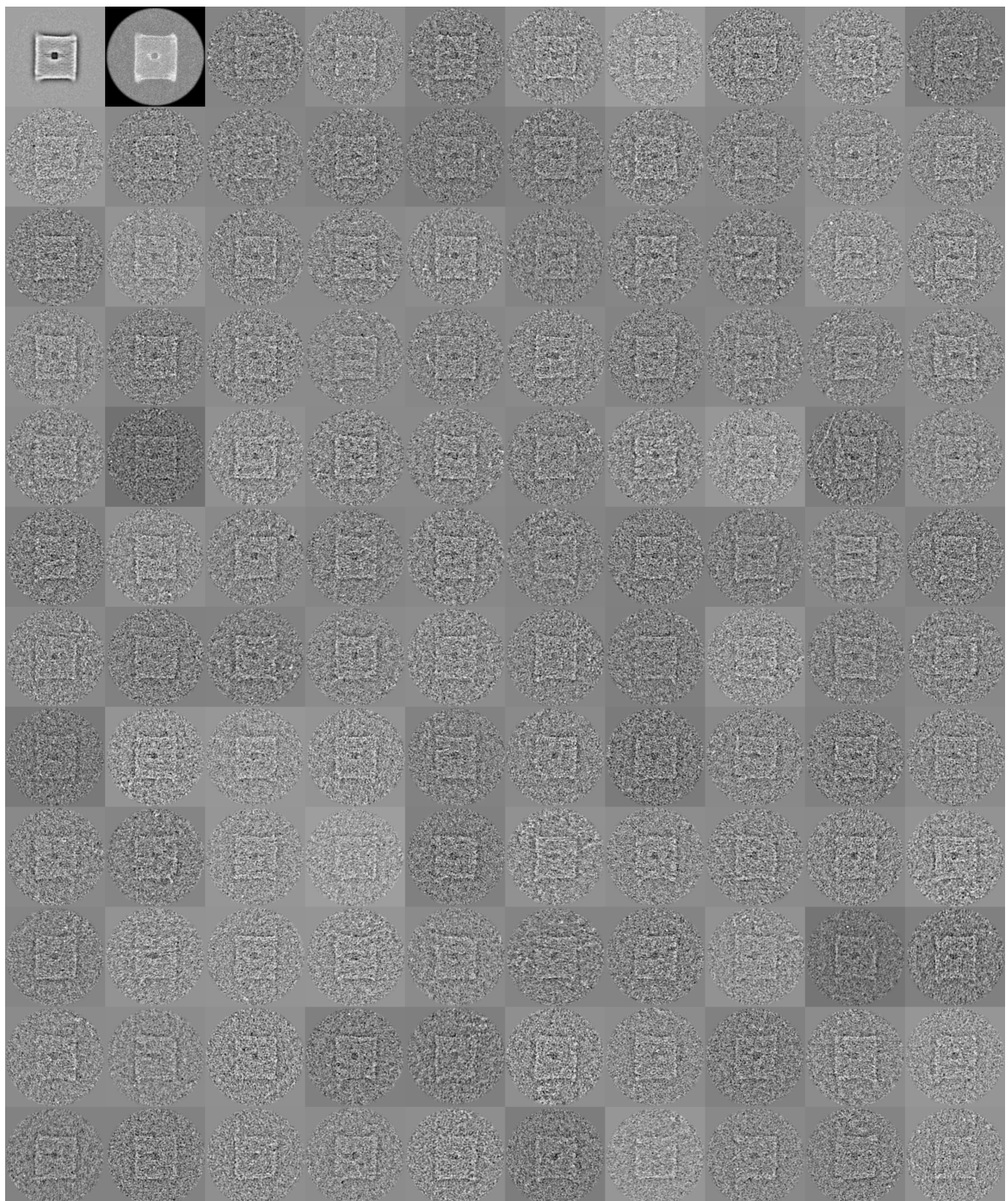


Fig. S8:

Negative-stain TEM micrographs of DNA nanoplate with 5nm x 7nm aperture without loop. Scale of each micrograph: 125nm x 125nm. Top row, image #1 = average micrograph; image #2 = variance micrograph computed from the shown library of micrographs.

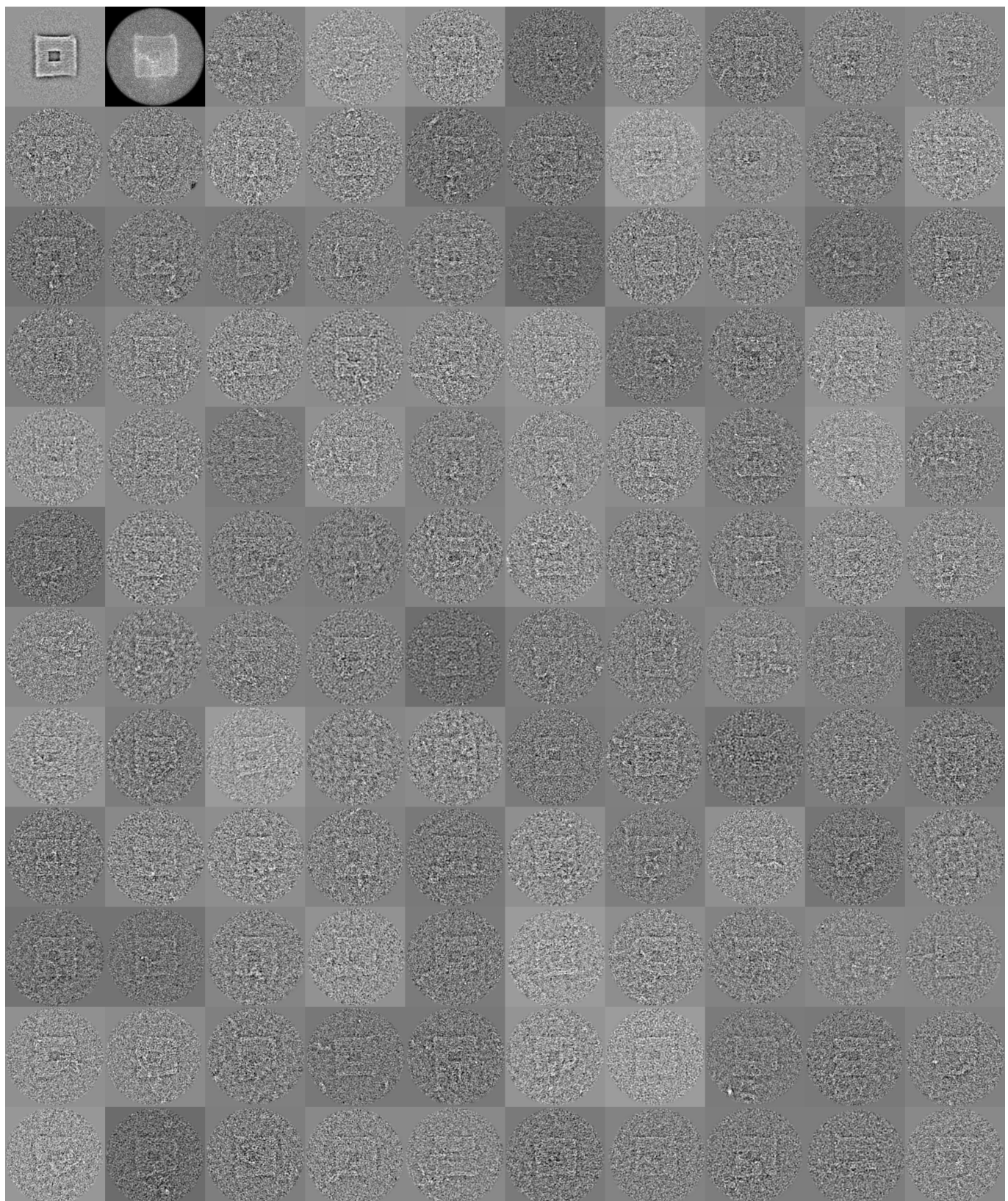


Fig. S9:

Negative-stain TEM micrographs of DNA nanoplate with 9nm x14 nm aperture. The flexible loop occurs in random orientations relative to the gatekeeper plate. Scale of each micrograph: 125nm x 125nm. Top row, image #1 = average micrograph; image #2 = variance micrograph computed from the shown library of micrographs.

Note S2: SiN nanopore fabrication and experimental methods

SiN nanopore fabrication.

Nanometer-sized holes in free-standing 50 nm thick SiN membranes were fabricated as previously described [5]. Briefly, the nanopores were patterned in the top SiN layer of the supporting wafer (180 μ m thick silicon coated with 50nm SiN on both sides) using electron beam lithography (e-Line system by Raith GmbH; 30keV acceleration voltage; 10 μ m aperture; ZEP520A resist) and reactive ion etching (CF₄ gas; 3.40min). A square window (320x320 μ m²) was created in the bottom SiN layer using optical lithography and reactive ion etching. Finally, wet chemical etching in aqueous potassium hydroxide solution (KOH; 20% w/w; 80° C; ~3h) etched away the exposed silicon and released the free-standing top SiN layer containing the nanopore. The diameter of the nanopore could be controlled precisely by variation of the electron beam dose during exposure (typically 1fC for pores with 25nm diameter). The pore diameters were analyzed using transmission electron microscopy (Philipps CM100; operated at 100kV).

Electrical measurement setup.

For electrical measurements, the nanopore chip was passivated with polydimethylsiloxane (PDMS) by manually applying PDMS around the membrane in order to reduce electrical noise of the chip [6]. Immediately before mounting the nanopore chips in the measurement chamber, the chips were exposed to oxygen plasma for 30s on both sides in a plasma cleaner (TePla-100E) in order to remove organic contaminants and to facilitate pore wetting. Subsequently, the chip was installed between two compartments (*cis* and *trans*) of the custom-built measurement chamber that were each filled with 400 μ L degassed and filtered electrolyte solution (1M KCl; 11mM MgCl₂; 0.5xTBE buffer at pH 8.0). Two silver / silver-chloride (Ag/AgCl) electrodes were immersed from the top into the electrolyte compartments. Bias voltages were applied to the *trans* side electrode and the ionic currents through the nanopore were recorded using a patch-clamp amplifier (HEKA EPC8). All current traces were recorded with a sampling frequency of 200kHz and a 10kHz low-pass Bessel filter.

DNA nanoplate capture and translocation experiments.

DNA nanoplates were captured onto the SiN nanopores by adding ~30pM nanoplates to the *cis* side chamber and then applying a positive bias voltage (up to +230mV) to the *trans* side electrode while recording the current. The captured nanoplate could be removed again by applying a negative bias voltage (up to -500mV), by thoroughly rinsing the chip or by an oxygen plasma treatment (30s on both sides). For translocation experiments, first the analyte was added to the *cis* side and analyte translocations through the bare SiN pore were recorded at constant positive bias voltages. Then, nanoplates were also added to the *cis*

side and after a nanoplate was captured at a positive bias voltage, analyte translocations through the hybrid nanoplate/nanopore structure were recorded. Recombinant streptavidin, monoclonal rat IgG_{2a} antibody and 6kbp dsDNA were purchased from Rockland Immunochemicals, AbD Serotec and Fermentas, respectively. Recombinant M13mp18 filamentous bacteriophage genomic DNA (7249 bases) was prepared as previously described [3]. 50mer short oligonucleotides (T_{50} , T_{24} -CC- T_{24} and T_{23} -CCGG- T_{23}) were synthesized by Eurofins MWG Operon (Ebersberg, Germany). Current traces of translocation experiments were analyzed using a Matlab pulse detection algorithm [7] with respect to pulse height and pulse width.

Note S3: Current noise analysis

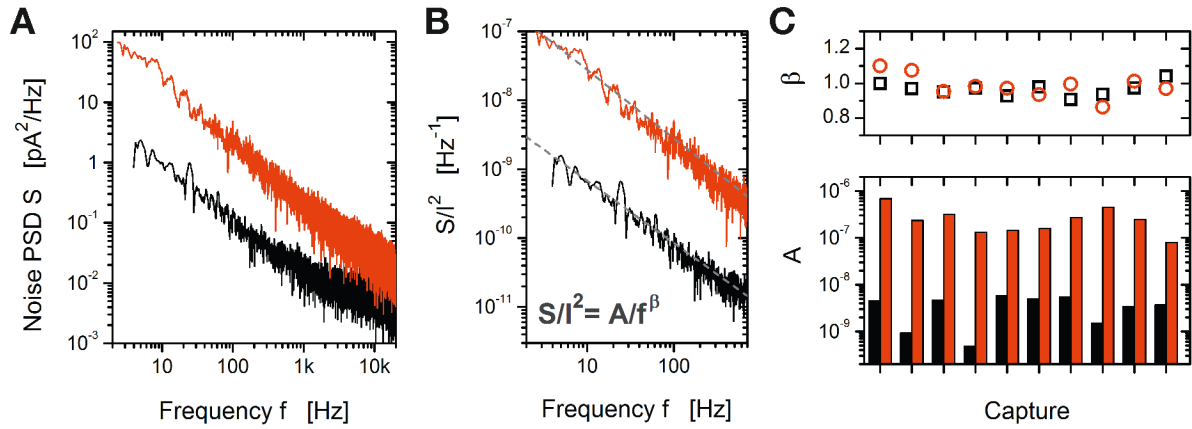


Figure S10. Current noise analysis of the nanoplate-on-nanopore hybrids. **(A)** Noise power spectral density of a bare 25nm SiN nanopore before (black) and after incorporation of a DNA nanoplate with a central 5x7nm aperture (red). Current traces were recorded at 230mV with a 10kHz low-pass Bessel filter. **(B)** Normalized current power spectral density in the low frequency range. Grey dashed lines are fits to Equation S1. **(C)** Extracted values of noise power and the exponent for 10 different SiN nanopores (diameters ~25nm) before (black) and after incorporation of a DNA nanoplate.

Noise of the ionic current in solid-state nanopores has been extensively studied in the past [6, 8-10]. As seen in Figure 1C, the current noise increases upon capture of a DNA origami plate. Noise power spectral densities $S(f)$ were obtained by performing Fast-Fourier Transformations of recorded current traces. Figure S10A compares the noise power spectra of a nanopore before and after capture of a nanoplate. Clearly, there is increased noise in the low frequency range. Low frequency current fluctuations have been previously observed in all solid-state nanopores [6, 8, 11] and are typically described as

$$\frac{S}{I^2} = \frac{A}{f^\beta} \quad (\text{S1})$$

where I is the current, S/I^2 is the normalized current noise power spectral density, f is the frequency, A denotes the noise power, and β the exponent of the scaling of the power spectra.

Figure S10B shows the normalized noise power spectral density S/I^2 at low frequencies of the bare nanopore and after incorporation of a nanoplate. The data were fitted using Equation S1 as shown by the dashed grey lines. We analyzed the normalized noise power spectra before and after nanoplate capture for 10 different nanopores and the fitted values for the exponent β and the noise power A are depicted in Figure S10C. The exponent β is in all

measurements close to 1 both before and after incorporation of the nanoplate ($\beta = 0.96 \pm 0.04$ for bare nanopores and $\beta = 0.99 \pm 0.06$ for nanoplate-on-nanopore hybrids). The power A of this 1/f noise, however, typically increases by two orders of magnitudes upon capture of the nanoplate. There is also variability in the noise power from nanopore to nanopore by one order of magnitude: for bare nanopores A ranges from 4.7×10^{-10} to 5.7×10^{-9} and for the nanoplate-on-nanopore hybrid from 7.9×10^{-8} to 6.9×10^{-7} . We attribute the increased current noise of the nanoplate-on-nanopore hybrid to additional 1/f noise. The origin of the 1/f noise in nanopores has not been fully understood, but Hooge's phenomenological relation [8, 11, 12] explains the observed current fluctuation as a result of mobility fluctuation. Other reported hybrid nanopore systems such as SiN nanopores coated with lipid layers [13] or nucleoporins [14] also exhibit higher 1/f noise than bare SiN pores.

Note S4: Influence of nanopore diameter on nanoplate capture, nanopore arrays

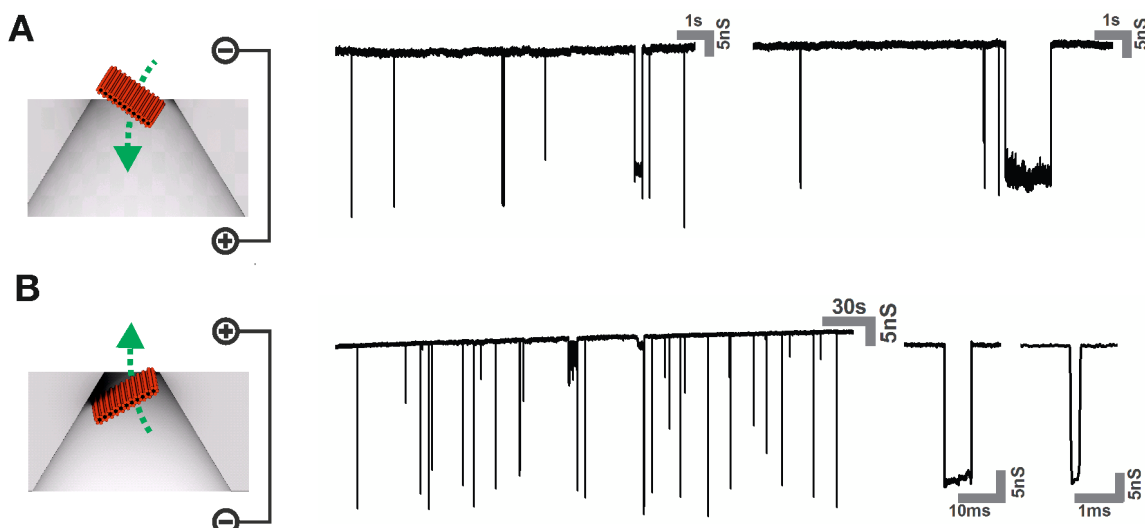


Figure S11. Influence of nanopore diameter and orientation on nanoplate capture. (A) DNA nanoplates translocate through a SiN nanopore with diameter $D=50$ nm. (B) DNA nanoplates translocate through a SiN nanopore with diameter $D=38$ nm when injected to the trans side of the SiN membrane at reversed voltage bias.

We investigated the influence of the SiN nanopore diameter and orientation on the success in capturing an DNA nanoplate. Our SiN nanopores feature a conical shape with sidewalls angled at 70° and a small tip diameter D [5]. Figure S11A demonstrates that nanopores with diameters larger than the dimension of the nanoplate could not stably capture a nanoplate. Instead, only current dips indicating translocation of the nanoplate through the nanopore could be detected. We also find that the orientation of the nanopore is crucial to successful capture of a nanoplate: even for a nanopore with diameter smaller than the nanoplate's lateral dimensions, no stable capture could be observed when the nanoplates were added to the side of the large nanopore opening (Figure S11B).

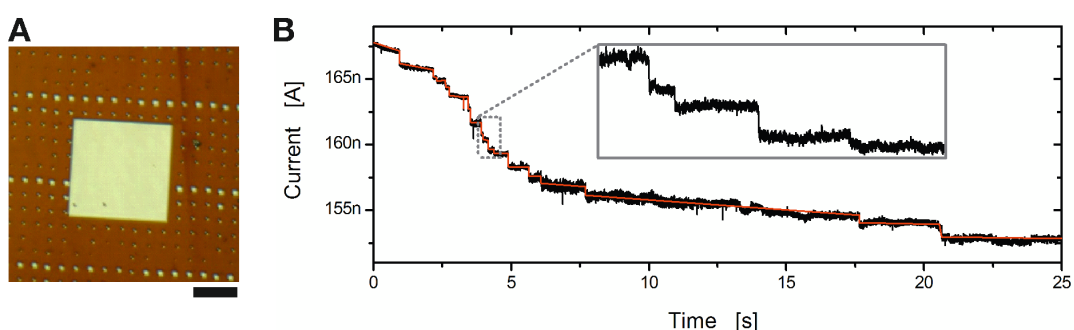


Figure S12. (A) Optical micrograph of a nanopore array chip. The membrane (large white square) contains $7 \times 7 = 49$ nanopore with diameter ranging from 20nm to 50nm. Black scale bar is $20\mu\text{m}$. **(B)** Progressive capture of nanoplates onto individual pores as indicated by staircase-like current decrease.

Note S5: Conductance of the DNA nanoplate on SiN nanopore hybrid

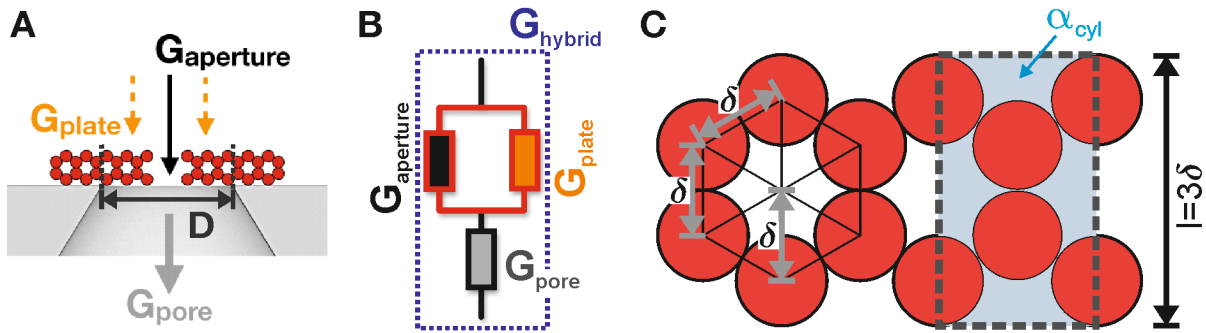


Figure S13. Conductance model of the nanoplate-on-nanopore hybrid. **(A)** Schematic model, **(B)** equivalent circuit of the nanoplate-on-nanopore hybrid. **(C)** Schematic cross-section of the DNA nanoplate where the cross-sections of individual DNA double-helices are shown as filled circles.

The assembly of a DNA nanoplate on top of a SiN nanopore is accompanied with an abrupt drop in the measured *trans* nanopore current (cf. Fig. 1C). In Fig. 1D we show the relative change in conductance $G_{\text{hybrid}}/G_{\text{pore}}$ where G_{hybrid} and G_{pore} denote the measured conductances before and after DNA nanoplate assembly on the nanopore. The decrease in conductance caused by assembly of nanoplates lacking any aperture onto nanopores is $\sim 17\%$, which points to additional ion fluxes through the DNA nanoplate itself. Figure S13A depicts schematically the involved conductances for a nanoplate-on-nanopore hybrid. The corresponding equivalent circuit is shown in Figure S13B, where the nanopore conductance G_{pore} is in series with two conductances due to fluxes through and underneath the DNA nanoplate itself, G_{plate} , and through the central aperture, G_{aperture} . The total conductance G_{hybrid} is then

$$G_{\text{hybrid}} = \left(\frac{1}{G_{\text{pore}}} + \frac{1}{G_{\text{aperture}} + G_{\text{plate}}} \right)^{-1} \quad (\text{S2})$$

The conductance of the apertures G_{aperture} can be estimated from its width x , height y , and depth l (cf. Fig. 1A) and the conductivity κ of the electrolyte solution as

$$G_{\text{aperture}} = \kappa \cdot \frac{xy}{l} \quad (\text{S3})$$

In a 1M KCl solution with 11mM MgCl₂ ($\kappa = 11 \text{ S/m}$), the conductance G_{aperture} of the aperture alone is 64 nS for $x=5\text{nm}$ and $y=7\text{nm}$ and 231 nS for $x=9\text{nm}$ and $y=14\text{nm}$. Using these values for G_{aperture} together with the measured conductances G_{pore} and G_{hybrid} allows for computing G_{plate} by re-arranging equation S2.

$$G_{plate} = \left(\frac{1}{G_{hybrid}} - \frac{1}{G_{pore}} \right)^{-1} - G_{aperture} \quad (S4)$$

Fig. 1G depicts the thus calculated values G_{plate} versus the measured conductance of the bare nanopore G_{pore} . The plot clearly demonstrates a linear correlation between G_{plate} and G_{pore} . The conductance G_{pore} of a SiN nanopore of diameter D and length L itself can be estimated:

$$G_{pore} = \kappa \cdot \frac{\pi D^2}{4L} \quad (S5)$$

Hence, the experimentally observed proportionality between G_{plate} and G_{pore} suggests that the conductance of the DNA nanoplate G_{plate} is governed by transverse current flow through the plate area directly above the SiN nanopore. DNA nanoplates with differing aperture sizes all exhibit the same linear dependence on the nanopore area. All points in Figure 1G lie approximately on the same fit line:

$$G_{plate} = (5.9 \pm 0.2) \cdot G_{pore} \quad (S6)$$

The specific conductivity of the nanoplate ρ_{plate} can be computed from $\rho_{plate} = \pi D^2 / (4l \cdot G_{plate})$, which gives a value of $\rho_{plate} = 7.8 \pm 0.4 \text{ S/m}$. We now compare our experimental results for the DNA nanoplate conductance to a simple geometric conductance model that considers the volume excluded by double-helical DNA domains in a DNA nanoplate. The nanoplates consist of double-helical DNA domains arranged in parallel in a honeycomb-type lattice packing (Fig. S13C). If each of the DNA double-helices in the nanoplate was a solid cylinder, the filled volume fraction would be around 60%. Yet, each of the double-helical DNA domains only fill a fraction of the volume taken up by an envelope cylinder. We estimate the fill factor dsDNA/cylinder to be around 0.5. Hence the total volume fraction f occluded by DNA in the DNA nanoplates is approximately $f=0.3$. Assuming that only currents through fraction of the nanoplate that is directly above the nanopore contribute to the conductance of the nanoplate we estimate G_{plate} via equation S7:

$$G_{plate} = (1 - f) \cdot \kappa \cdot \frac{\pi D^2}{4l} \quad (S7)$$

Using Equation S5 we find that

$$G_{plate} = (1 - f) \cdot \frac{L}{l} \cdot G_{pore} = 5.3 \cdot G_{pore} \quad (S8)$$

Therefore, the relationship between G_{plate} and G_{pore} that we find with our simple geometric model agrees quite well with the experimentally observed relationship (Equation S6).

Note S6: Analysis of streptavidin translocations

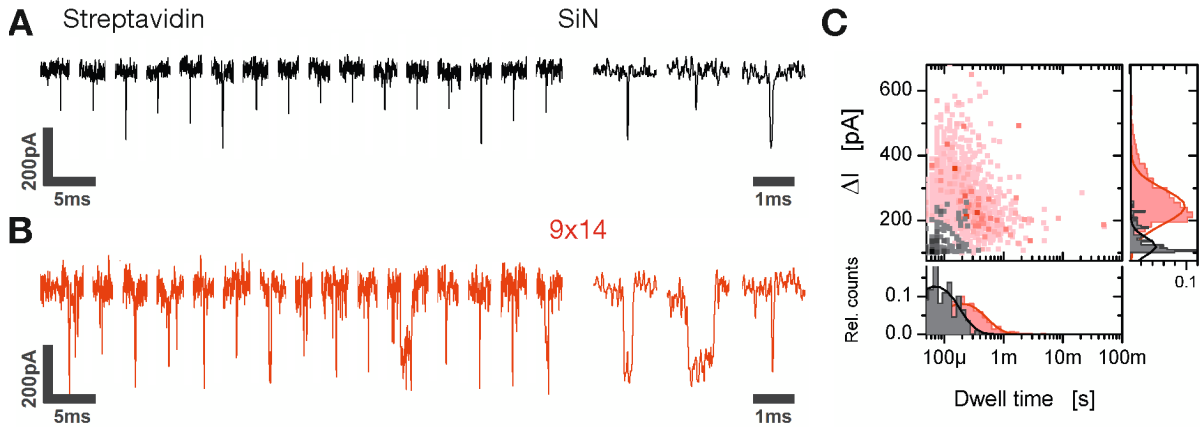


Figure S14. Streptavidin translocations at 200mV bias voltage. **(A)** Representative events through the bare nanopores. **(B)** Representative events through a nanoplate-on-nanopore hybrid with central 9nmx14nm aperture. **(C)** Scatter plot comparing streptavidin translocations through bare SiN pore (grey) and nanoplate-on-nanopore hybrid (red). Solid lines in the histograms of the peak amplitudes are Gaussian fits. Solid lines in the logarithmically binned histograms of the dwell times are fitted using a single-exponential distribution (Equation S9).

Figure 2 shows continuous current-time traces of streptavidin translocation through a bare SiN nanopore (Fig. 2A) and through a nanoplate-on-nanopore hybrid with a 9nmx14nm central aperture (Fig. 2B). A magnified set of representative translocation events are shown in Fig. S14A and 14B. The amplitude ΔI and dwell time t of each individual event is extracted using the Matlab peak finding algorithm. Fig. S14C depicts a scatter diagram in which each translocation event is plotted with its amplitude versus its dwell time. We find that streptavidin translocates the bare SIN nanopore with an average amplitude of $\Delta I = (120 \pm 23)\text{pA}$ and an average apparent dwell time of $\tau = (70 \pm 12)\mu\text{s}$.

After incorporation of the DNA nanoplate, both the amplitude and the dwell time of streptavidin translocation increases: $\Delta I = (244 \pm 54)\text{pA}$ and $\tau = (202 \pm 20)\mu\text{s}$. Note that the increase in amplitude results from the increase in dwell time: streptavidin quickly translocates through the bare nanopore and therefore the pulses are significantly attenuated in amplitude by the employed 10kHz low-pass filter [7] (ie. pulses do not reach a bottom plateau, cf. magnified view in Figure S14A). In the case of the nanoplate-on-nanopore hybrid with a the smaller aperture as compared to the bare nanopore opening, many translocation events last longer and can therefore develop a bottom plateau (cf. Figure S14B). Similar findings have been reported for DNA translocation through very small SiN pores [15].

Note S7: Analysis of dsDNA translocations

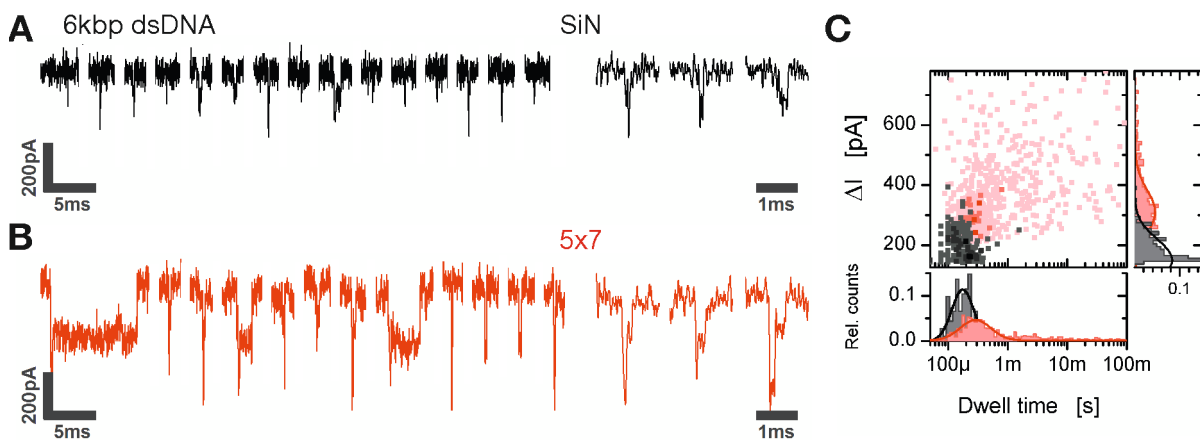


Figure S15. Double-stranded DNA (6kbp) translocations at 200mV bias voltage. **(A)** Representative events through the bare nanopore. **(B)** Representative events through a nanoplate-on-nanopore hybrid with central 5nmx7nm aperture. **(C)** Scatter plot comparing dsDNA translocations through bare nanopore (grey) and nanoplate-on-nanopore hybrid (red). Solid lines in the histograms of the peak amplitudes are Gaussian fits. Solid lines in the logarithmically binned histograms of the dwell times are fitted using a single-exponential distribution (Equation S9).

Figure 2 shows continuous current-time traces of double-stranded DNA translocation through a bare nanopore (Fig. 2G) and through a nanoplate-on-nanopore hybrid with a central 5nmx7nm aperture (Fig. 2H). A magnified set of representative translocation events are shown in Figure S15A and 15B. A scatter diagram is depicted in Figure S15C. We find that dsDNA translocates through the bare nanopore with $\Delta I = (150 \pm 64)\text{pA}$ in $\tau = (211 \pm 24)\mu\text{s}$. After incorporation of the nanoplate, both the amplitude and the dwell time of the translocations increase to $\Delta I = (311 \pm 72)\text{pA}$ in $\tau = (400 \pm 29)\mu\text{s}$. In contrast to streptavidin translocations, most of the dsDNA events are long enough to be fully resolved (magnified views in Figure S15A and B). The longer dwell times for the case of nanoplate-on-nanopore hybrids with the small 5nmx7nm aperture is in accordance with previous reports [15] where small SiN nanopores ($D \sim 4\text{nm}$) yielded longer lasting and more complex dsDNA translocations.

Note S8: DNA nanoplate without central aperture

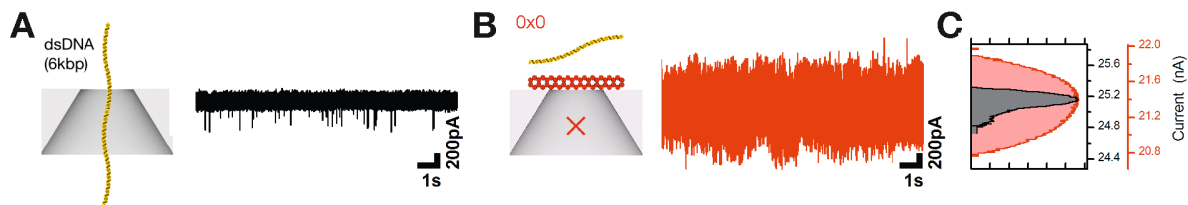


Figure S16. Inhibition of DNA translocation using a DNA nanoplate without aperture. **(A)** Current-time trace of 6kbp dsDNA (300pM) translocations through a bare SiN nanopore. **(B)** Current-time trace after insertion of a DNA origami nanopore with no central aperture. **(C)** Histograms of observed current levels.

Figure S16 shows a representative translocation control experiment with a DNA nanoplate lacking a central aperture on a SiN nanopore. While the dsDNA translocated through the bare nanopore, translocations could not be observed after the a nanoplate was assembled onto the SIN nanopore.

Note S9: M13mp18 genomic DNA in a nanoplate without bait motif

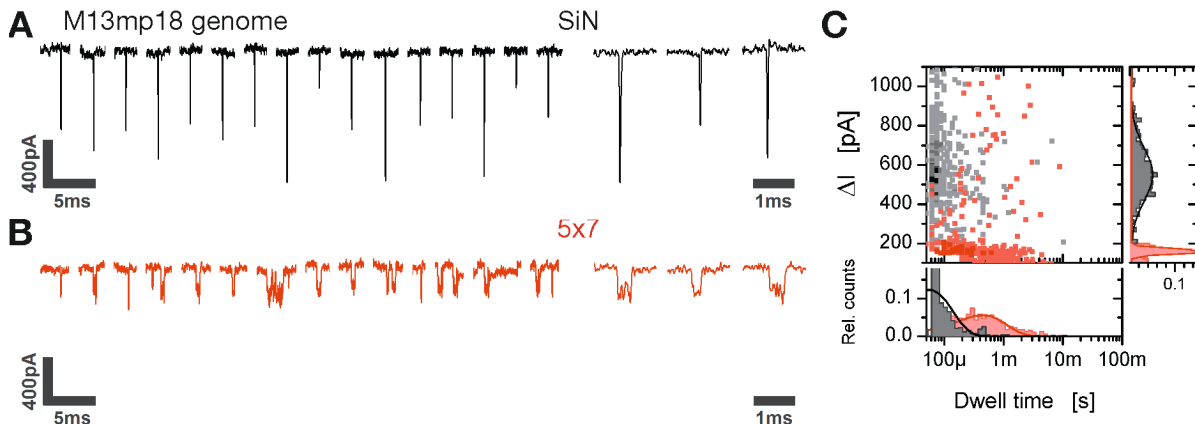


Figure S17. Translocations of M13mp18 genomic DNA. **(A)** Representative events observed with the bare SiN nanopore. **(B)** Representative events observed with a nanoplate-on-nanopore hybrid with central 5nmx7nm aperture without bait motif. **(C)** Scatter plot comparing M13mp18 DNA translocations through bare nanopore (grey) and nanoplate-on-nanopore hybrid (red). Solid lines in the histograms of the peak amplitudes are Gaussian fits. Solid lines in the logarithmically binned histograms of the dwell times are fitted using a single-exponential distribution (Equation S9).

Representative translocation events observed with the M13mp18 genomic DNA (circular, single-stranded DNA of length 7249 bases forming complex secondary structure (see inset Fig 3F) through a bare nanopore and through a nanoplate-on-nanopore hybrid with central 5nmx7nm aperture without any bait motif are shown in Figure S17A and S17B, respectively. The corresponding scatter diagram is depicted in Figure S17C. Remarkably, events caused by the M13mp18 DNA for the case of the bare SiN nanopore induce very short blockades $\tau=(54\pm10)\mu\text{s}$ with greater current reductions $\Delta I=(522\pm135)\text{pA}$ than translocations of double-stranded DNA through a comparable nanopore (cf. Figure S15A). This observation is in accordance with a recent study [16] and is caused by the fact that the M13mp18 likely traverses the nanopore ($D\sim25\text{nm}$) as a globular coil and therefore causes a large current blockade. In the smaller aperture of the DNA nanoplate, however, the M13mp18 molecule has to uncoil in order to pass through and hence we observe longer $\tau=(444\pm31)\mu\text{s}$ but smaller $\Delta I=(160\pm18)\text{pA}$ current blockades.

Note S10: M13mp18 genomic DNA in a nanoplate with multiple bait motifs

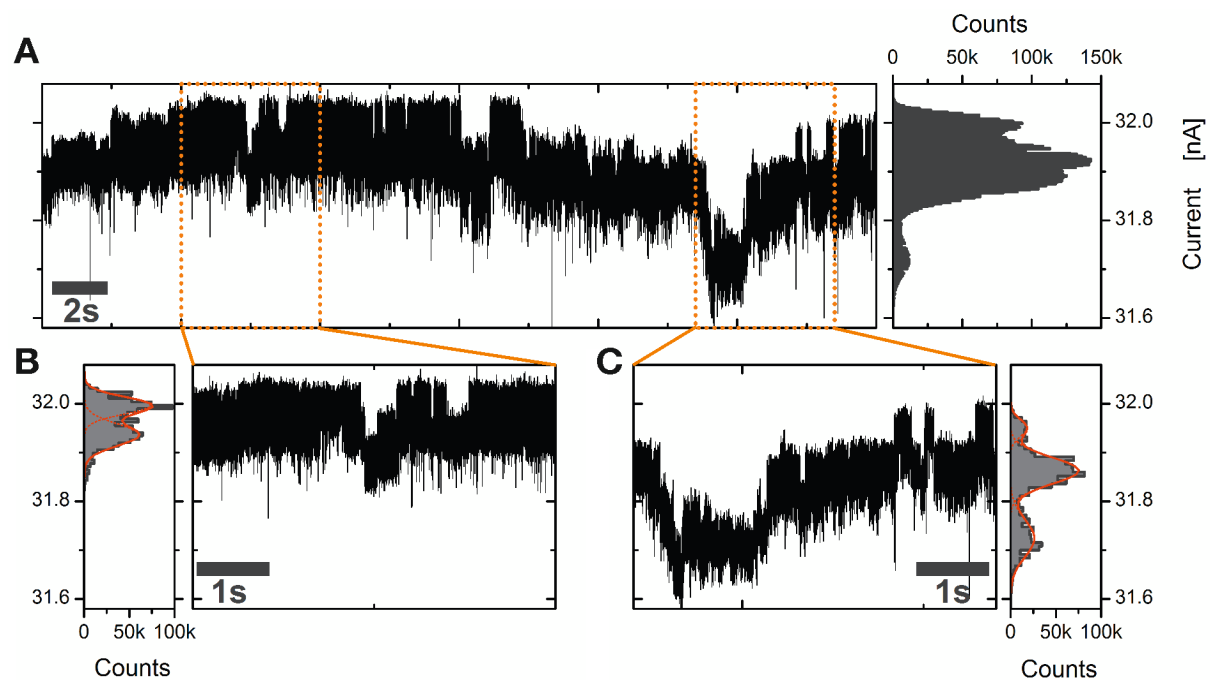


Figure S18. **(A)** Current-time trace and current histogram observed for the M13mp18 genome in a nanoplate-on-nanopore hybrid with six bait motifs of sequence ‘TTTAATT’ bound to the central 5nm \times 7nm aperture. **(B,C)** Zoom-ins on two time segments. Current histograms are fitted with multi-Gaussian peaks.

Complex, multi-level current blockades indicate that multiple segments of individual M13mp18 DNA molecules can simultaneously enter, dwell in, and leave the nanoplate aperture. The dwells are induced by adhesion of multiple single-stranded portions of the M13mp18 to the multiple bait motifs in the aperture.

Note S11: M13mp18 genomic DNA in nanoplate: dwell time analysis

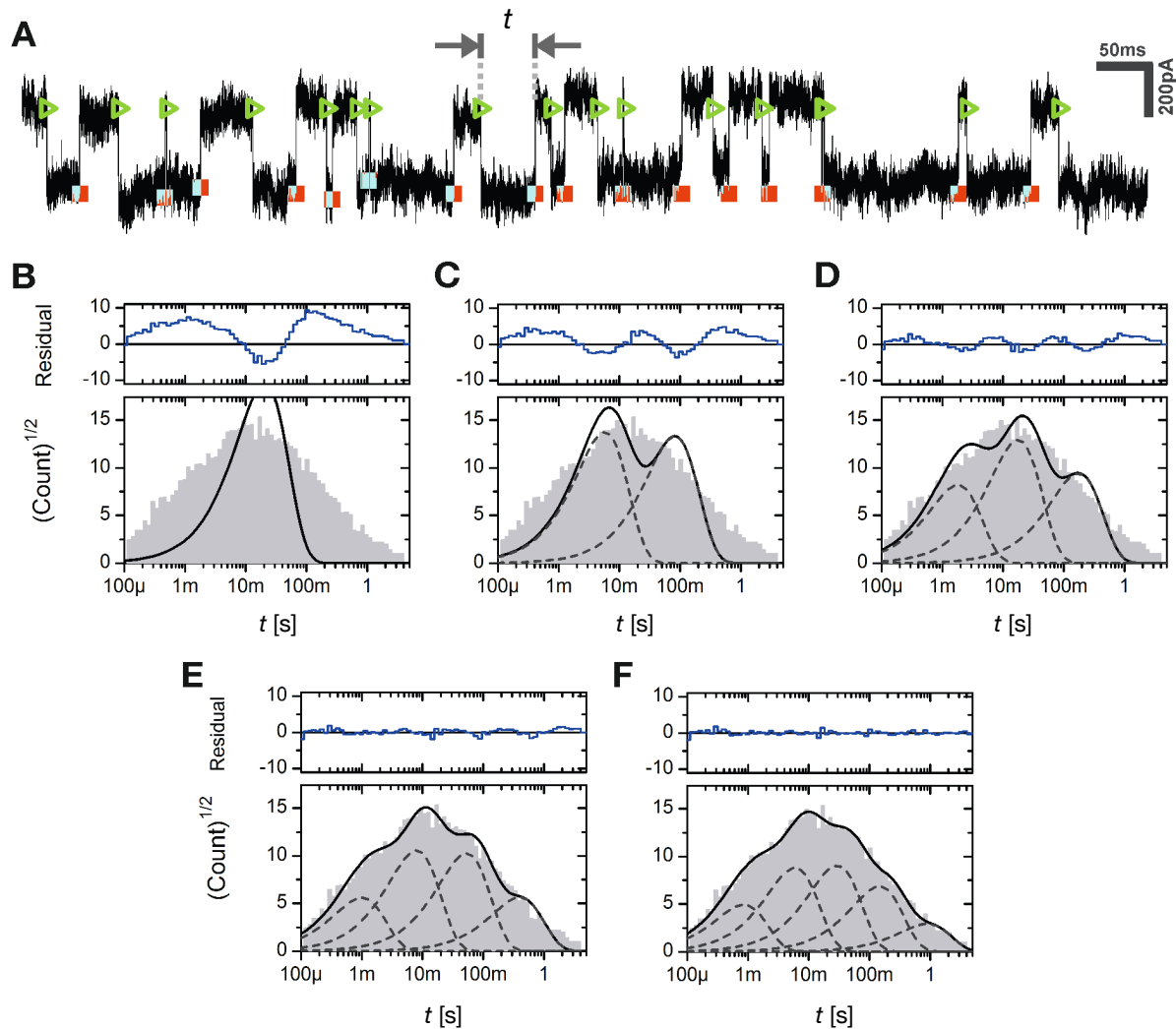


Figure S19. M13mp18 genome in a nanoplate-on-nanopore hybrid with aperture-bound ‘TTTAATT’ bait motif. **(A)** Exemplary current-time trace. Green and red points mark the start and end points of the pulse as analyzed from the pulse detection algorithm. The dwell time t indicates the duration of each pulse. **(B-F)** Histograms of the dwell time distribution. Solid lines are multiple-exponential fits (Equation S10) with one (B), two (C), three (D), four (E) and five (F) components to logarithmically binned data. The fit residuals are shown in the upper insets.

For the translocation of the M13mp18 genome through a nanoplate-on-nanopore hybrid with aperture bound TTTAATT bait motif we observed distinct two-state current switching behavior (cf. Figure S19A). We attribute each event in the low current state to the presence of a segment of M13mp18 molecules in the aperture. The dwell time t is the duration of each binding event and can be extracted for each individual event using a pulse detection algorithm that we have implemented using MatLab.

A popular method to analyze the distributions of dwell times in single ion-channel recordings is to use constant logarithmic bin widths [17, 18]. With the transformation $x=\ln(t)$,

a single exponential distribution $P(t)$ with the characteristic time τ_{off} for the probability $P(t)dt$ for recording dwell time events within intervals dt around t transforms into a distribution $P(x)$ dx as follows:

$$P(t) \propto \exp\left(\frac{-t}{\tau_{off}}\right) \xrightarrow{x=\ln(t)} P(x) \propto \frac{1}{\tau_{off}} \exp\left(x - \frac{1}{\tau_{off}} \cdot \exp(x)\right) \quad (\text{S9})$$

An additive superposition of exponential distributions with characteristic time constants $\tau_{off,i}$ transforms into:

$$P(t) \propto \sum_i A_i \cdot \exp\left(\frac{-t}{\tau_{off}}\right) \xrightarrow{x=\ln(t)} P(x) \propto \sum_i A_i \cdot \frac{1}{\tau_{off,i}} \exp\left(x - \frac{1}{\tau_{off,i}} \cdot \exp(x)\right) \quad (\text{S10})$$

In Figure S19B-F, we fitted the dwell time distribution of the M13mp18 genome using multiple exponential components. A satisfying fit is reached only when using a minimum of five different exponentials. The five characteristic time constants $\tau_{off,0}=(0.8\pm0.1)\text{ms}$; $\tau_{off,1}=(5.9\pm0.5)\text{ms}$; $\tau_{off,2}=(29.6\pm3.5)\text{ms}$; $\tau_{off,3}=(146.0\pm17.8)\text{ms}$; $\tau_{off,4}=(898.7\pm138.8)\text{ms}$ are plotted in Figure 3G.

Note S12: Supporting References

1. Douglas, S.M., Marblestone, A.H., Teerapittayanon, S., Vazquez, A., Church, G.M., Shih, W.M., Rapid prototyping of 3D DNA-origami shapes with caDNAno. *Nucleic Acids Res*, 2009 (37): p. 5001-5006
2. Douglas, S.M., Dietz, H., Liedl, T., Hogberg, B., Graf, F., Shih, W.M., Self-assembly of DNA into nanoscale three-dimensional shapes. *Nature*, 2009 (459), p. 414-418
3. Castro, C.E., Kilchherr, F.K. et al, A primer to scaffolded DNA origami. *Nat Meth*, 2011 (3): p. 221-229
4. Tang, G., Peng., L., Baldwin, P.R., Mann, D.S., Jiang, W., Rees, I., Ludtke, S.J., EMAN2: an extensible image processing suite for electron microscopy. *J Struct Biol*, 2007 (157): p. 88-46
5. R. S. Wei, D. Pedone, A. Zurner, M. Doblinger, U. Rant, Fabrication of Metallized Nanopores in Silicon Nitride Membranes for Single-Molecule Sensing. *Small* **6**, 1406 (Jul, 2010).
6. V. Tabard-Cossa, D. Trivedi, M. Wiggin, N. N. Jetha, A. Marziali, Noise analysis and reduction in solid-state nanopores. *Nanotechnology* **18**, 6 (2007).
7. D. Pedone, M. Firnkes, U. Rant, Data Analysis of Translocation Events in Nanopore Experiments. *Anal. Chem.* **81**, 9689 (2009).
8. R. M. M. Smeets, U. F. Keyser, N. H. Dekker, C. Dekker, Noise in solid-state nanopores. *Proc. Natl. Acad. Sci. U. S. A.* **105**, 417 (2008).
9. J. D. Uram, K. Ke, M. Mayer, Noise and bandwidth of current recordings from submicrometer pores and nanopores. *ACS Nano* **2**, 857 (2008).
10. D. P. Hoogerheide, S. Garaj, J. A. Golovchenko, Probing Surface Charge Fluctuations with Solid-State Nanopores. *Phys. Rev. Lett.* **102**, 4 (Jun, 2009).
11. R. M. M. Smeets, N. H. Dekker, C. Dekker, Low-frequency noise in solid-state nanopores. *Nanotechnology* **20**, 4 (2009).
12. F. N. Hooge, 1/f noise is no surface effect. *Phys. Lett. A* **29**, 139 (1969).
13. E. C. Yusko et al., Controlling protein translocation through nanopores with bio-inspired fluid walls. *Nat. Nanotechnol.* **6**, 253 (Apr, 2011).
14. S. W. Kowalczyk et al., Single-molecule transport across an individual biomimetic nuclear pore complex. *Nat. Nanotechnol.* **6**, 433 (Jul, 2011).
15. M. Wanunu, J. Sutin, B. McNally, A. Chow, A. Meller, DNA Translocation Governed by Interactions with Solid-State Nanopores. *Biophys. J.* **95**, 4716 (Nov, 2008).
16. S. W. Kowalczyk, M. W. Tuijtel, S. P. Donkers, C. Dekker, Unraveling Single-Stranded DNA in a Solid-State Nanopore. *Nano Lett.* **10**, 1414 (Apr, 2010).
17. F. J. Sigworth, S. M. Sine, Data Transformations for Improved Display and Fitting of Single-Channel Dwell Time Histograms. *Biophys. J.* **52**, 1047 (Dec, 1987).
18. D. Colquhoun, in *Microelectrode Techniques; the Plymouth Workshop Handbook*, D. C. Ogden, Ed. (Company of Biologists, Cambridge, 1994), pp. 101-139.

Note S13
Sequence information

Staple strand sequences for DNA nanoplate without aperture.

Staple strand sequences for DNA nanoplates with 5nm x 7nm aperture lacking a flexible loop.

Staple strand sequences for DNA nanoplate with 5nm x 7nm aperture and a single bait motif.

Staple strand sequences for DNA nanoplate with 5nm x 7nm aperture and six bait motifs.

Staple strand sequences for DNA nanoplate with 9nm x 14nm aperture.

Staple strand sequences for forming a double-stranded loop for DNA nanoplate with 5nm x 7nm aperture.